UNIVERSITÀ DEGLI STUDI DI PADOVA

DIPARTIMENTO DI FISICA E ASTRONOMIA GALILEO GALILEI

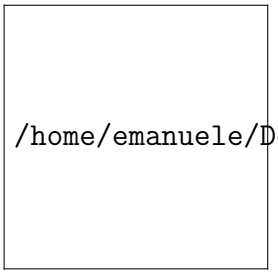

CORSO DI STUDI IN FISICA

Study of trigger efficiency for finding states of supersymmetric Higgs boson at LHC with CMS experiment

RELATORE: Prof. Ugo Gasparini
CORRELATORE: Dr. Stefano Lacaprara

LAUREANDO: Emanuele Michielin

26 Settembre 2012
Anno Accademico 2011-2012

Contents

Introduction

The *Compact Muon Solenoid* (CMS) experiment is a particle physics detector installed in the *Large Hadron Collider* (LHC). LHC is the world's largest and highest energy particle accelerator, designed to collide opposing particle beams of either protons or heavy ions at up to 7 TeV per beam for an energy of 14 TeV at center-of-mass with an ultimate designed luminosity of $10^{34}\ cm^{-2}s^{-1}$.

It was built to allow physicists to test the origin of masses in the Standar Model and in particular the existence of the Higgs boson and to test physics beyond the Standar Model at the TeV scale, such as supersymmetry[1], which predicts the existence of a large number of new particles. On 4^{th} July 2012 both CMS and ATLAS collaborations announced the discovery of a particle consistent with the Higgs boson in the mass region around $125-126$ GeV/c^2[2, 3]. Although this particle has properties compatible with those expected for the Standar Model Higgs boson, it is still possible that it is something different. We will know more in November/February with larger statistics. So far there is no evidence of any supersymmetric Higgs boson or any other new physics beyond Standar Model.

The goal of this thesis is to study the efficiency of the trigger used by the CMS group of Padova to search for states of supersymmetric Higgs boson. The trigger system reduces the event rate from about $20MHz$ to about $400Hz$. It is necessary because there is no technology capable to store such a quantity of data as that produced by all the inhelastic proton-proton collisions. So it is essential to know how many "good events" are lost, namely the efficiency of the trigger. A good knowlegde is mandatory for any physical result, e.g. for cross section measurements.

The structure of the CMS experiment and of the trigger system will be briefly described in the first chapter. In the second chapter the characteristics of the dataset, such as the trigger paths selections, the prescales and some distributions will be analyzed and finally, in the third chapter, the trigger efficiency will be measured.

Chapter 1

The CMS detector

There are four experiments installed at LHC interaction point: CMS, ATLAS, Alice and LHCb. This thesis uses data collected by CMS[4], a general purpose particle detector which studies all interesting events produced by the collision of the p-p and heavy ions beams. One of its peculiarities is the identification of muons and the accurate measure of their characteristic, useful for the research of rare particle. The main goal of the experiment is the exploration of physics phenomena at the TeV scale: to discover the Higgs boson and to study its properties and to look for evidence of physics beyond the standard model, such as supersymmetry.

The other general purpose experiment, ATLAS, is placed at the opposite side of the LHC ring and has similar goals. The two experiments are designed to complement each other, extend their reach and to provide corroboration of findings.

1.1 The detector structure

The CMS experiment has a cylindrical structure coaxial to the beam pipe with a diameter of 14.6 m and a length of 21.6 m for a total weight of 12500 $Tons$. As shown in Figure 1.1 the detector is divided into a central cylindrical region (barrel), segmented into five rings (wheels) along the beam direction(the z-axis of the CMS reference frame), and two discs at the ends (endcaps). A strong magnetic field of 3.8 T is necessary for accurate measurement of the transverse momentum of charged particles, and is provided by a solenoid superconducting magnet. The flux is returned through an iron yoke which is also the absorber of the spectrometer for the muons measurement.

The interaction point is the point in the center of the detector around which proton-proton collisions occur and it is also the center of the system

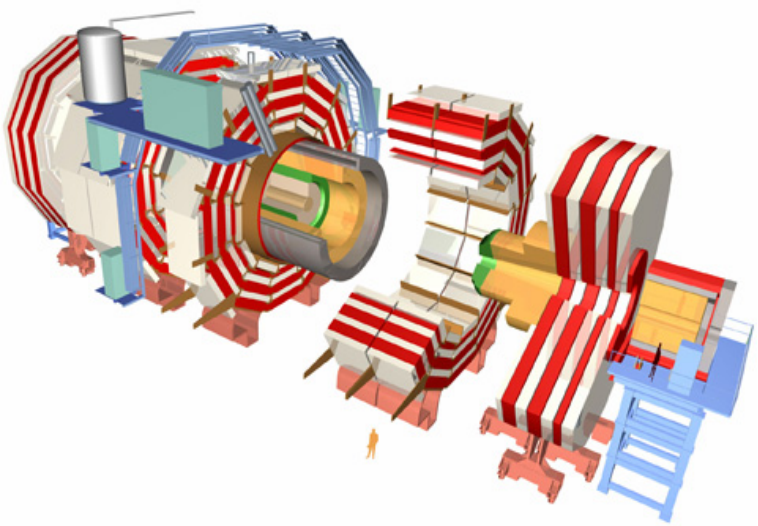

Figure 1.1: The CMS detector.

of coordinates. The system of coordinates commonly used is the cylindrical one, due to the cylindrical symmetry of the apparatus. The distance from the beam axis is r, φ is the azimuth angle and η is the pseudorapidity, defined as:

$$\eta = -\log\Big(\tan\Big(\frac{\vartheta}{2}\Big)\Big) \tag{1.1}$$

where ϑ is the polar angle. The pseudorapidity is preferred over the polar angle because it is invariant under relativistic boost and particle production is almost constant as a function of it .
CMS contains four main subsystems: the tracker, the electromagnetic calorimeter (ECAL), the hadronic calorimeter (HCAL) and the muon detectors. The first is immediately around the interaction point and is used to identify the tracks of charged particles and the vertices of interaction. Since a very good spatial resolution and efficiency is needed, the tracker consists in a pixel detector in the inner volume and in a silicon strip detector in the outer. This part of the detector is the world's largest silicon detector. It has 12 layers of silicons sensors for a total area of 205 m^2. The electromagnetic calorimeter is designed to measure with high accuracy the energies of electrons and photons; it is made of about 70.000 $PbWO_4$ scintillating crystals. The hadronic calorimeter is designed both to measure the energy of jets of hadronic particles such as protons, neutrons, pions and kaons and to be as hermetic as possible to allow the measurement of momentum imbalance in the transverse plan. It is composed of layers of dense material (brass) interleaved with tiles

of plastic scintillators. Outside the magnet there are 3 types of gaseous detectors used as muon detectors: drift tube chambers (in the barrel), cathode strip chambers (in the endcaps), and resistive plate chambers (both in the barrel and the endcaps). This setup is used for precise trajectory measurements and fast trigger of the muons. A schematic view of a slice of the CMS detector in the plane perpendicular to the beam direction is shown in Fig 1.2.

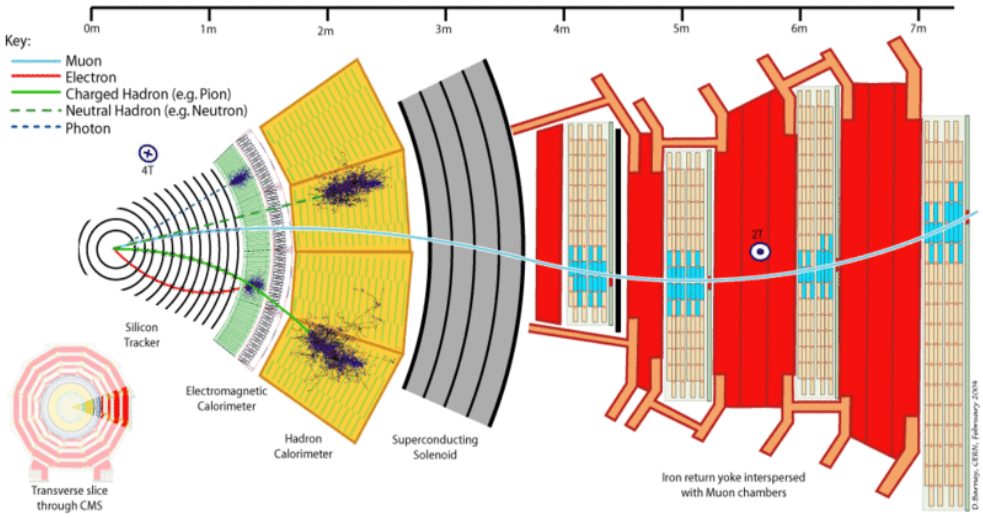

Figure 1.2: A slice of the CMS detector. From the left are shown the silicon tracker, the ECAL, the HCAL, the superconducting solenoid and the muon chambers. Five sample tracks of five different particles are shown.

1.2 The trigger system

To have a good chance of producing a rare particle, such as a Higgs boson, a very large number of collisions is required. LHC provides a bunch collision rate of 20 MHz. Most of these collision events are "soft" and do not produce interesting phenomena. Each event has a raw data size of approximately 200 KB, which, at the 20 MHz crossing rate, would result in 0.4 TB of data per second, an amount that the experiment cannot store or even process properly.

So, one of the most important and difficult aspects of the experiment is the design of the trigger system, providing real-time selection of the useful events. Sophisticated and fast selection algorithms are implemented, using

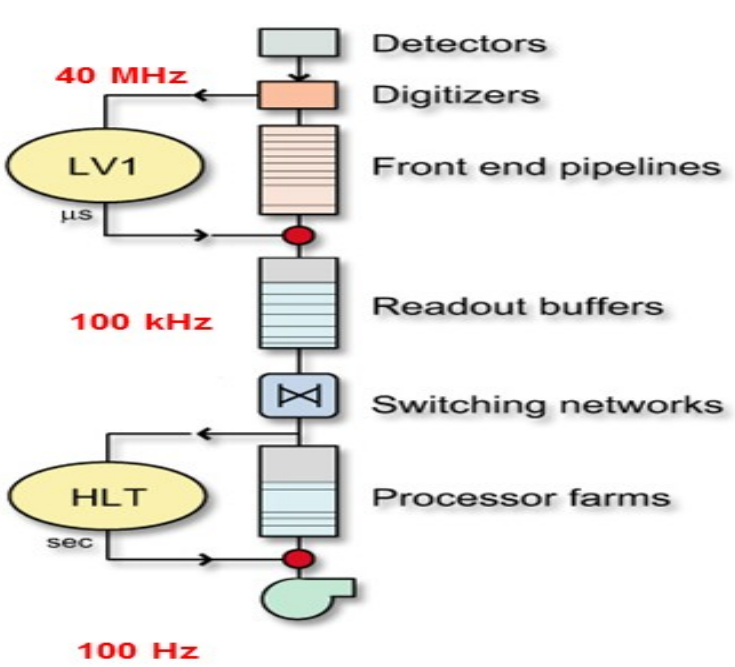

Figure 1.3: Scheme of the trigger system. The numbers refers to the original CMS design. Now the final output accapter is about 400 Hz

selective information from all the detector subsystems during real-time data taking. The CMS trigger is designed to perform a data reduction down to about 400 Hz using different sequential trigger levels, as shown in Fig. 1.3.

The first trigger level (*Level-1*), schematically shown in Fig. 1.4, is implemented on dedicated hardware devices. It uses the information of the muon system and of the ECAL and HCAL calorimeters, with reduced granularity with respect to the final data used in the reconstruction performed at later stage, reducing the data rate to about $100KHz$. Each event passing *Level-1* is sent to further levels that are software filters executed in a processor farm. This is the higher level of real-time data selection and is referred to as *High-Level Trigger* (HLT) in which the full detector information, including pixel and silicon strips tracker, is used. It reduces the data rate to about $400Hz$. Only data accepted by the *HLT* are recorded for off-line physics analysis.

To minimize the CPU required by the *HLT* a characteristic of the algorithms is to reconstruct the information only partially. In fact in many cases the decision on whether an event should be accepted by the *HLT* involves the reconstruction in only a limited region of the detector. As an example, for a muon event accepted by the *Level-1* trigger, only the parts of the muon chambers indicated by the *Level-1* and the corresponding track in the tracker

need to be studied for the validation and refinement of the muon candidate kinematical properties. This approach has a considerable advantage in terms of CPU and input/output. Moreover, rather sophistcated algorithms on reconstructed particles such those to identify b-quarks ("b-tagging" algorithms, see chapter 2) can be performed at HLT level.

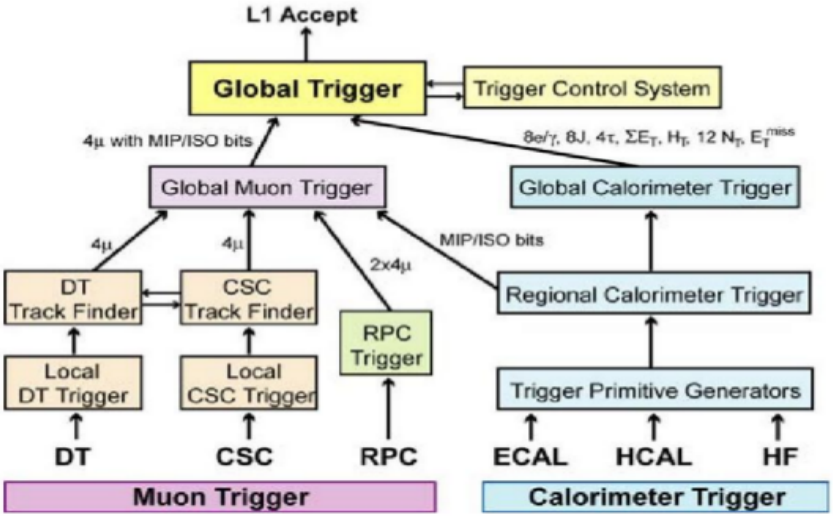

Figure 1.4: Scheme of the *Level-1* trigger system.

Chapter 2

Data analysis

The discovery of a particle of mass around 125-126 GeV/c^2, whose behaviour so far has been consistent with a Higgs boson, can be seen as a major success of the SM prediction or, if its features will be different from that predicted by SM, an evidence for new physics beyond current theories. A possible extension of the SM is the supersymmetry, which predicts a large set of new particles. In particular, in the minimal supersymmetric Standar Model there are two Higgs doblets originating five physical states: three neutral and a pair of charged. Neutral bosons states decay in 90% of the time into a bottom–antibottom quark pair, and can be produced in association with additional b quarks in the pp interaction $pp \to bbH$, $H \to b\bar{b}$, with a cross section which can be interesting for CMS sensitivity[7]. Therefore, a trigger with an on-line identification of b-quarks (b-tagging) is needed. Since the b-tagging algorithm is quite slow, other selections at trigger level are required in order to decrease the rate before applying the on-line b-tag. A muon and two jets, with thresholds on the transverse momentum and two b-tags, are the selections chosen for the trigger for the study of the $H \to b\bar{b}$ channel with a semi-leptonic final state.
The analysis presented in this thesis uses data collected by CMS in the period between April and August during the 2012 run, corresponding to an integrated luminosity of 9.38 fb^{-1} at a center of mass energy of 8 TeV.

In this analysis a "particle flow[5]" event reconstruction is used, based on the identification and reconstruction of individual particles in the event, obtained using a combination of all subdetectors information. Charged hadrons are reconstructuted combining information from tracker and calorimeters, electrons from tracker and ECAL, photons using ECAL only, neutral hadrons from HCAL and finally muons from tracker and muon chambers. For the search of states of supersymmetric Higgs boson in $H \to b\bar{b}$ channel, the features of the jets produced are of great importance. A jet is a narrow cone

of particles produced by the fragmentation of a quark or a gluon. Jet momentum is determined as the vector sum of all particle momenta in the jet. An other important feature of a jet is its flavour, in particular, if it has been produced by the fragmentation of a b quarks. The b-mesons are relatively long lived, so they travel for some distance (of the order of some mm) before decaying, resulting in a displaced secondary vertex or at least a set of tracks not pointing to the original primary vertex.

In this analysis a b-tagging algorithm , the "Combine Secondary Vertex[6]" (CSV), is used, which combines in a likelihood ratio the impact parameter significance of the tracks (the impact parameter divided by its error, where the impact parameter is the distance of closest approach of the reconstructed particle trajectory with respect the primary vertex) and the information of the secondary vertex and the jet kinematics to provide identification of jets originated from the fragmentation of b-quarks. The CSV returns a variable in the range between 0 and 1; the more close to 1, the higher is the probability that the jet is originated from a bottom quark. We refer as b-tagged jets the jets which have an associated CSV variable above a certain threshold. In this analysis the threshold is set to 0.8 for the first and the second jet. This implies a mistag (the probability that a jet which is not originated from a bottom quark is b-tagged) of about 1%.

2.1 Trigger paths

To collect data for the supersymmetric Higgs signal search, a quite complex trigger path is used. It requires a muon, two jets above 40 and 20 GeV/c respectively and two b-tags. In order to study this complex trigger path, a set of subsidiary paths have been developed, each relaxing or removing one of the requirement of the physical path in order to study its impact in term of efficiency.
The studied triggers paths are listed below. They all require a muon p_T above 10 GeV/c and jets reconstructed at Level-1.

Mu12 only requires a muon p_T above 12 GeV/c with a $|\eta| < 2.1$;
Mu12_DiJet20 requires a muon p_T above 12 GeV/c with a $|\eta| < 2.1$, two jets with a p_T threshold of 20 GeV/c;
Mu12_DiJet40_20 requires a muon p_T above 12 GeV/c with a $|\eta| < 2.1$, two jets with a p_T threshold of 40 and 20 GeV/c, respectively;
Mu12_DiJet40_20_BTag requires a muon p_T above 12 GeV/c with a $|\eta| < 2.1$, two jets with a p_T threshold of 40 and 20 GeV/c, respectively, and one on-line b-tag;

HLT paths	rate [Hz]	triggered events
Mu12	~ 0.8	1004855
Mu12_DiJet20	~ 0.4	529302
Mu12_DiJet40_20	~ 0.4	579001
Mu12_DiJet40_20_BTag	~ 0.4	589290
Mu12_DiJet40_20_DiBTag	~ 8	10050380

Table 2.1: HLT paths rates and number of triggered events. The rate is averaged over the data taking period.

Mu12_DiJet40_20_DiBTag requires a muon p_T above 12 GeV/c with a $|\eta| < 2.1$, two jets with a p_T threshold of 40 and 20 GeV/c, respectively, and two on-line b-tags. This trigger, unprescaled, is the one used for the physical analisys focused on the $H \to b\bar{b}$ search.

It is important to note that the off-line reconstruction and b-tagging is much more accurate than the one performed at on-line stage. This is a fundamental concept that will be better explained in Chapter 3.
Table 2.1 reports the total number of events recorded and the corresponding rates for the different trigger paths.

2.2 The pre-scale

All triggers, but Mu12_DiJet40_20_DiBTag, are pre-scaled, namely they do not accept all the events which pass the trigger algorithms but they accept only a pre-defined fraction of them. Pre-scaling is used to reduce the rate of the triggers with softer thresholds, otherwise would be impossible not to exceed the maximum rate of processable events, about 400 Hz. The prescaling factor changes (increases) with the increase of the instantaneous luminosity delivered by LHC, which increased in turn during 2012 thanks to improvement on the accelerator. Also, it changes during a fill of the LHC, when the instantaneous luminosity decreases following the protons reduction in the bunches. In this case, the pre-scale factor decreases in order to maintain the rate of every trigger as high as over the fill. For this reason, in order to work with unprescaled, we have to weight each event passing a trigger path with its pre-scale factor. Figure 2.1 shows how the instantaneous luminosity decreases following the protons reduction in the bunches, on the left for events triggered by our Level-1 trigger, on the right by our HLT trigger path. The rate decreases from about 11 KHz to about 400 Hz for the Level-1 and from

about 11 Hz to about 4 Hz for the our trigger path.

In Figure 2.2 the total rate Level-1 trigger is plotted as a function of time for a long run (about twelve hours). Is possible to see how the prescale is changed when the rate become low.

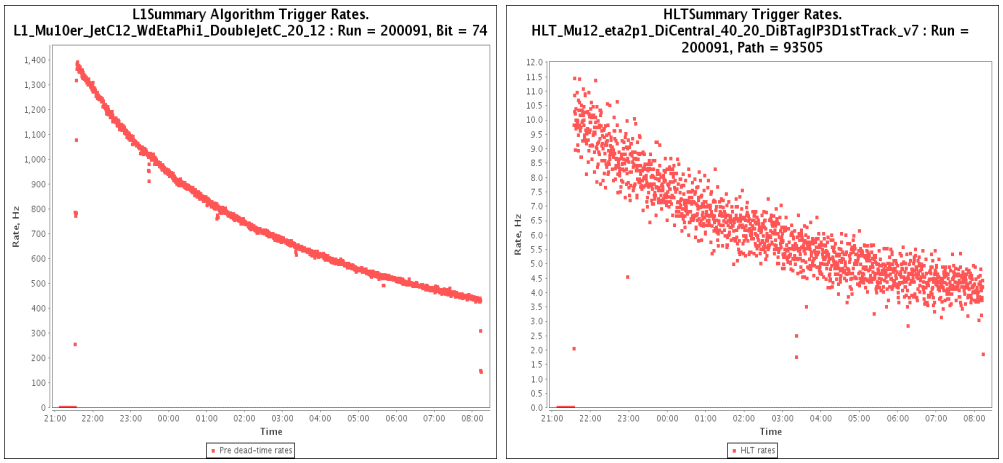

(a) Level-1 (b) HLT

Figure 2.1: The rate in function of the time for a Level-1 trigger (a) and for the Mu12_DiJet40_20_DiBTag trigger path (b).

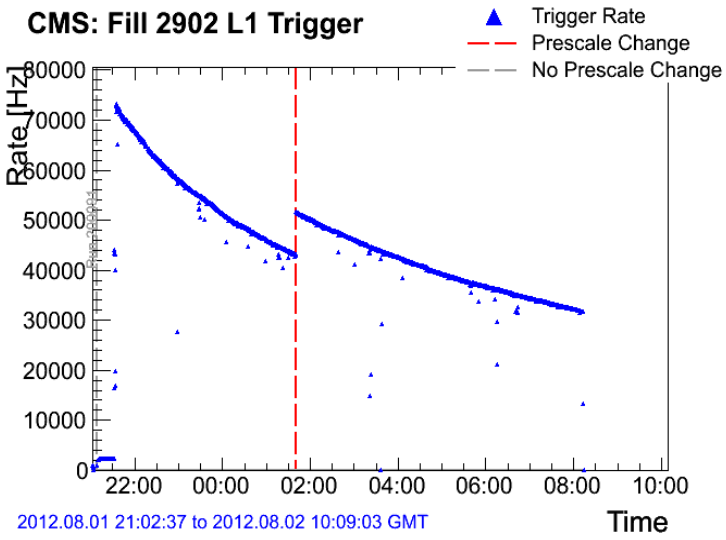

Figure 2.2: The rate in function of the time.

2.3 P_T, η and ϕ distribution

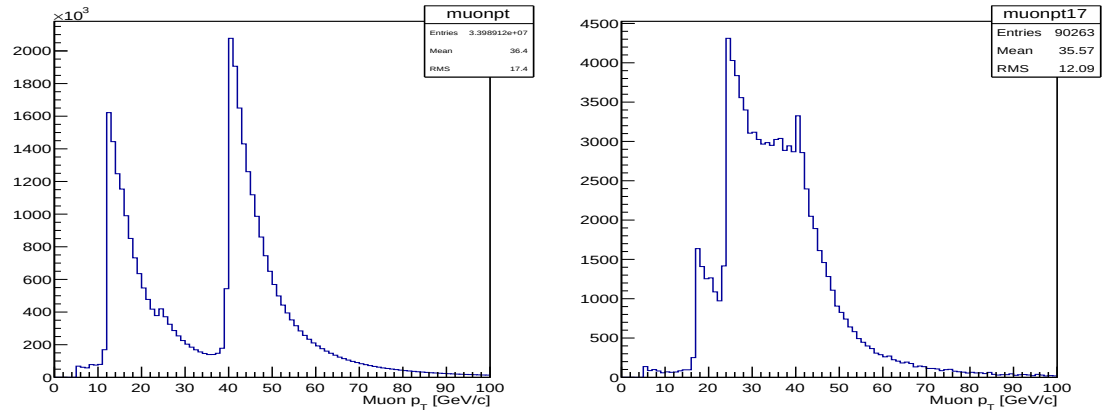

Figure 2.3: Left: p_T distribution of all muons. Right: p_T distribution of muons that have passed HLT_Mu17 trigger.

In Figure 2.3 two p_T distributions of the most energetic muon in the event are shown. On the left is plotted the distribution of all the events in the dataset. Four muons triggers, with thresholds set to 12, 24 and 40 GeV/c, are easily recognizable. The trigger with higher threshold (HLT_Mu40) is not prescaled, while the others are scaled by large factors. The reason is that the most populated region is the low-momentum one, but it is also the less interesting region for the search of new physics.

On the right it is shown the distribution of muon p_T, as reconstructed off-line, for all the muons accepted by the HLT_Mu17 trigger path. Below the threshold set to 17 GeV/c, there is a tail of accepted muons. These muons were reconstructed on-line with a p_T above 17 GeV/c, therefore they passed the trigger. Instead off-line, with a better reconstruction, they result to have a lower p_T. This fact will be studied in Chapter 3. The HLT_Mu24 trigger is clearly recognizable by the structure of this distribution. It can be noted that the HLT_Mu17 is prescaled by a larger factor than the HLT_Mu24 trigger path. In this Figure it is also possible to see a physical phenomenon. Around 35 GeV/c the exponential decrease of the distribution of the muons is slowed because of the muons generated in the decay of heavy vector bosons, $W \to \mu\nu$ and $Z \to \mu\overline{\mu}$, which have a mass of about 80 and 90 GeV/c^2, respectively. The peak at 40 GeV/c is an artefact of the unprescaled HLT_Mu40 path.

On the left of Figure 2.4 is shown the $|\eta|$ distribution of the muons. The hole visible around $\eta = 0.2$ is due to blind areas at the edges of the central

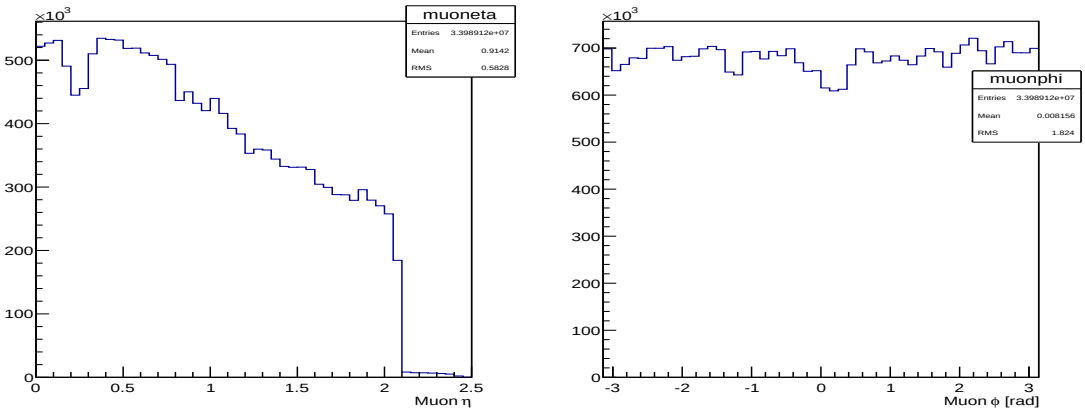

Figure 2.4: Left: η distribution of all muons. Right: ϕ distribution of all muons.

wheel. The decrease of the number of muons as $|\eta|$ increases is caused by the inverse proportionality between p_T and $|\eta|$. The sharp drop at 2.1 is due to the geometrical acceptance of the single muon trigger (while double muon triggers are accepted also in the most difficult region, covered by the muon chambers, up to $|\eta| = 2.4$). The ϕ distribution, shown in the right plot in the Figure, is uniform as expected.

In Figure 2.5 the off-line transverse momentum distributions of the leading jet (upper left plot) and of the sub-leading jet (upper right plot) are shown for all the triggered events, where the jets are sorted in descending order. The bottom plots in the Figure show the distribution of the transverse momentum of the leading jet (left) and the sub-leading jet (right) for the events accepted by the Mu12_DiJet40_20_DiBTag trigger path. It can be seen that the imposition of the jet p_T threshold, in this case at 40 GeV/c for the leading jet, does not result in a sharp p_T distribution in the corresponding off-line variable, as it was in the muon case. The reason is the difference between on-line and off-line jet reconstruction. At on-line level, only the calorimeters are used, while off-line also the tracker is used. So on-line and off-line jets are more different than the analogous muons objects.

The two dimensional plot of Figure 3.6 shows the angle ϕ of the first jet versus the angle ϕ of the second jet. It is clear that, in most events, the difference between the two angles is close to π. This is the physical consequence of four-momentum conservation in events with two-jets topology.

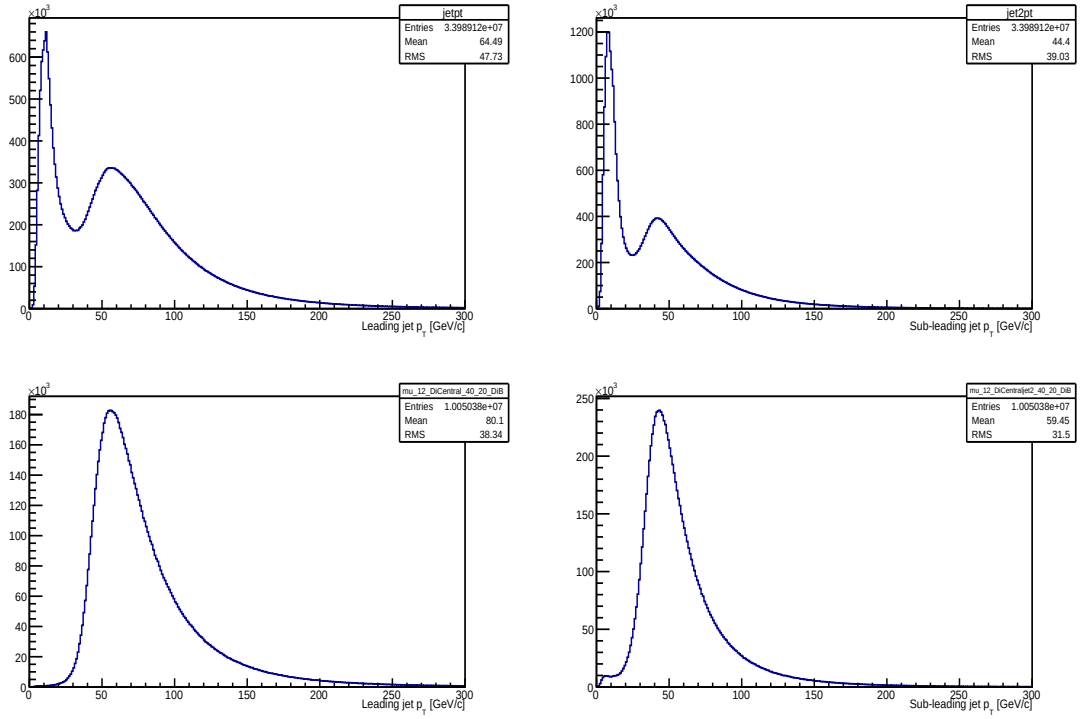

Figure 2.5: Jets p_T distribution

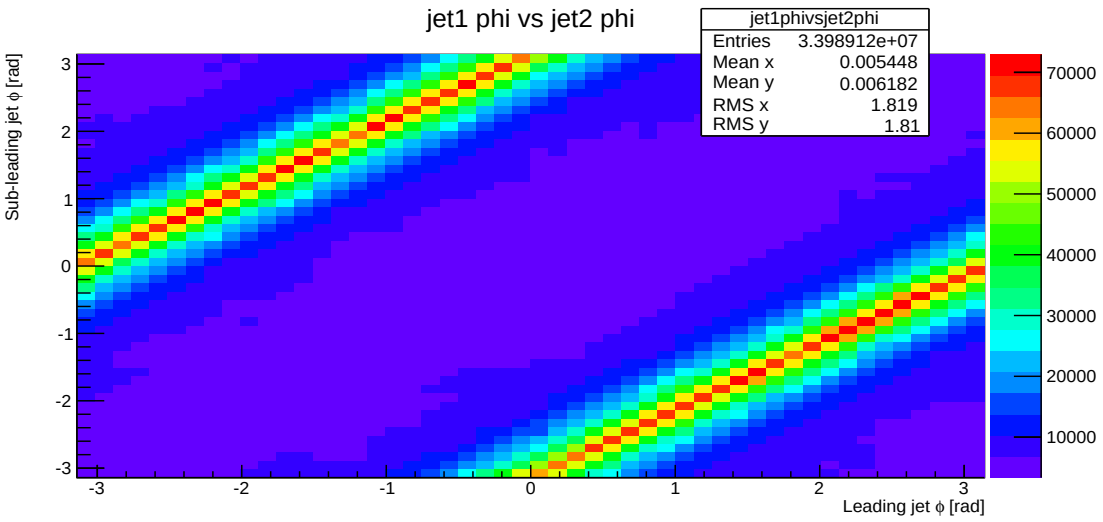

Figure 2.6: First jet ϕ vs second jet ϕ.

Chapter 3

Trigger efficiency

The main purpose of this analysis is to evaluate the efficiency of the Mu12_DiJet40_20_DiBTag trigger path, which is used for the physics analysis of the $H \to b\bar{b}$ process.
The best way would be to compare the data sample with an obtained by a unbiased trigger, but the events accepted by the random trigger would hardly be accepted also by the trigger with these tight selections. Then there would not be enough statistics for the analysis. A Montecarlo simulation can be used in order to obtain an unbiased data sample, but, having the possibility, it is better to use real CMS data.

In this thesis a data driven analysis has been performed. The trigger efficiency has been evaluated considering the off-line reconstruction as the correct reproduction of the physical quantities. In fact off-line jet reconstruction is much better than on-line, as seen in section 2.4. Also on-line b-tagging is performed by looking only at the impact parameter significance of the tracks associated to a given jet. No secondary vertex is searched for, unlike the off-line CSV algorithm.

The trigger paths presented in section 2.2 are used to find the Mu12_DiJet40_20_DiBTag efficiency. The first trigger path only requires a muon p_T above 12 GeV/c. The next one requires a harder selection, in this case two jets with a p_T threshold of 20 GeV/c. Once the efficiency of the second trigger with respect to the first one is found, the trigger efficiency for the two jets can be evaluated. Adding a harder selection step by step, we can "build" our trigger and find its final efficiency as the convolution of the efficiency of each of its thresholds.

3.1 Turn-on curves

The turn-on curve is the trigger efficiency as a function of the p_T. It is obtained from the ratio between the data sample passing the trigger with tighter selection and the one with softer selection.
For example for the inclusive muon trigger with threshold set to 40 GeV/c HLT_Mu40 the turn-on curve (Figure 3.1) is defined as:

$$\epsilon_\mu = \frac{N(HLT\_Mu40 \ \wedge \ HLT\_Mu\_less\_40)}{N(HLT\_Mu\_less\_40)} \tag{3.1}$$

where HLT_Mu_less_40 is the result of the logical OR of inclusive muon triggers with threshold less to 40 GeV/c. For the other trigger paths is not necessary to calculate the logical AND in the numerator being each a strict subset of the previous one. This also simplifies the calculation having to take into account the prescales. The unprescaled number of events triggered by Mu12_DiJet20 and Mu12_DiJet40_20, N_{20} and N_{40}, can be evaluated as follow:

$$N_{20} = N_{20}^{PS} * PS^{20} \qquad N_{40} = N_{40}^{PS} * PS^{40} \tag{3.2}$$

where N_{20}^{PS} is the number of events passing the prescaled Mu12_DiJet20 trigger path and N_{40}^{PS} is the number of events passing the prescaled Mu12_DiJet40_20 trigger path, we can write:

$$\frac{N^{40} \ \wedge \ N^{20}}{N^{20}} = \frac{N^{40}}{N^{20}} = \frac{N_{40}^{PS} * PS^{40}}{N_{20}^{PS} * PS^{20}} \tag{3.3}$$

The same argument applies to the other triggers.

Good performance of a path is indicated by a steep beginning of the curve, a high value of the efficiency at the nominal threshold cut and a high plateau level.

Figure 3.1 shows the turn-on curve of the HLT_Mu40 trigger path as function of the reconstructed muon transverse momentum. For technical reasons the turn-on curve for HLT_Mu12 is not shown. So the "muon step" is not formally justified. But, as can be seen in Figure 3.1, the muon triggers efficiencies have a steep beginning and a plateau level very close to 1. Figs 3.2-3.5 show the trigger efficiency of each trigger path, calculated relative to the previous one as function of reconstructed leading and sub-leading jet transverse momentum.
Figure 3.2 shows the efficiency of Mu12_DiJet20 trigger. Unlike the curve of the muon (Fig 3.1) the beginning of the curve is not very steep. This because jets are objects much more complicated than the muons. Events which were wrongly reconstructed on-line with a p_T above the threshold, at off-line stage

result with a lower p_T.
In Figure 3.3 the efficiency of Mu12_DiJet40_20 trigger is shown. The value where the trigger reaches 50% efficiency is at around 50 GeV/c for the leading and around 40 for the sub-leading jet, although the difference between the two set thresholds is 20 GeV/c. This because sometimes a jet reconstructed as leading on-line is then reconstructed as sub-leading at off-line level and vice-versa.
Figure 3.4 shows the efficiency of Mu12_DiJet40_20_BTag trigger, while in Figure 3.5 the efficiency of Mu12_DiJet40_20_DiBTag trigger is plotted. An off-line CSV b-tag discriminator $CSV > 0.8$ is required for both leading and sub-leading jet for the Mu12_DiJet40_20_BTag efficiency computation, whereas, in addition to the $CSV > 0.8$ for both leading and sub-leading jet, a $CSV > 0.7$ is required for the third jet for the Mu12_DiJet40_20_DiBTag efficiency. The requirement of off-line $CSV > 0.8$ for the leading and for the sub-leading jet are added in order to ensure that at least two b-jets are indeed present in the event, otherwise the plot would return the rate of b-tagged jets in the data sample.
Figure 3.4 shows the efficiency of the on-line b-tagging with respect to the off-line b-tagging. It can be seen an expected relation between the b-tagging and the transverse momentum of the jet: the lower is the transverse momentum the lower is the efficiency. In fact a jet with a high p_T is easier to reconstruct and to obtain a better resolution of the secondary vertex. Figure 3.5 shows the efficiency of the double on-line b-tagging with respect to the triple off-line b-tagging. It is worse than those for the single b-tag on-line efficiency because we are asking that two out of three jets have on-line b-tagging, not one out of two as in the case of Fig. 3.4.

The curves have been then fitted with the following function:

$$f(x) = \frac{[p0]}{2}\Big(1 + Erf\Big(\frac{x - [p1]}{[p2]}\Big)\Big) \tag{3.4}$$

where Erf(x) is the error function defined as the integral between 0 and x of the Gaussian function, [p0] is the plateau value, [p1] denotes the value where the trigger reaches 50% efficiency and [p2] is the width of the turn-on curve.

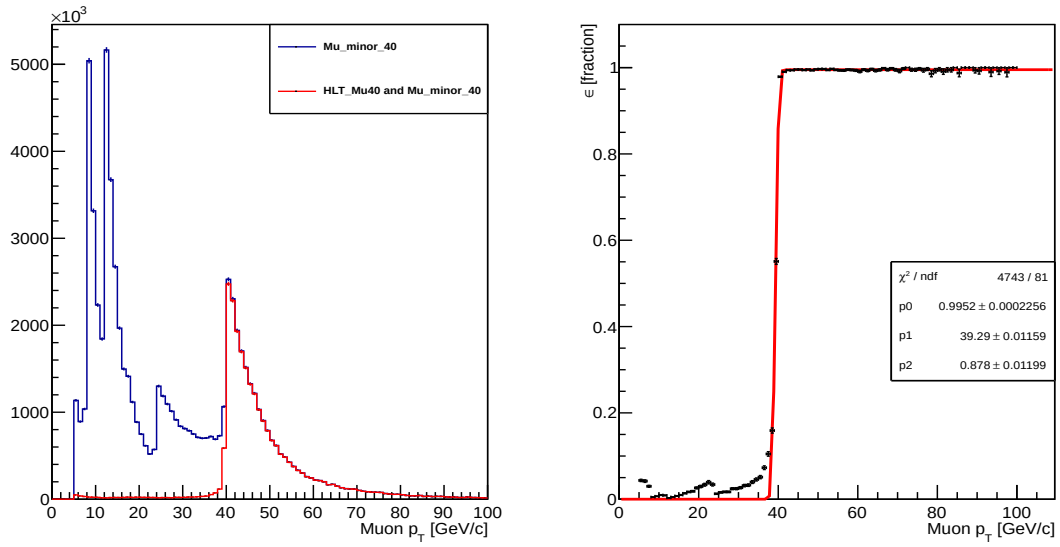

Figure 3.1: Left: reconstructed transverse momentum distribution of the muon in events triggered by HLT_Mu40 (red) and HLT_Mu_less_40 (blue). Right:trigger efficiency of the HLT_Mu40 trigger path as function of the reconstructed muon.

3.2 Conclusions

Using data collected by the CMS experiment at the LHC from *pp* collisions at 8 TeV centre-of-mass energy, the hadronic Mu12_DiJet40_20_DiBTag trigger efficiency have been evaluated.
For the leading jet, for the values equal to 46 and 61 GeV/c, where the trigger reaches the 50% and 90% of efficiency in the Mu12_DiJet40_20 turn-on, the total hadronic trigger efficiency results equal to 0.209 ± 0.014 and 0.555 ± 0.029 respectively.
For the sub-leading jet, for the values equal to 33 and 51 GeV/c, where the trigger reaches the 50% and 90% of efficiency in the Mu12_DiJet40_20 turn-on, the total hadronic trigger efficiency results equal to 0.1934 ± 0.013 and 0.490 ± 0.029 respectively.
These results will be used by the CMS group of Padova for the search for states of supersymmetrical Higgs boson in the 2012 dataset.

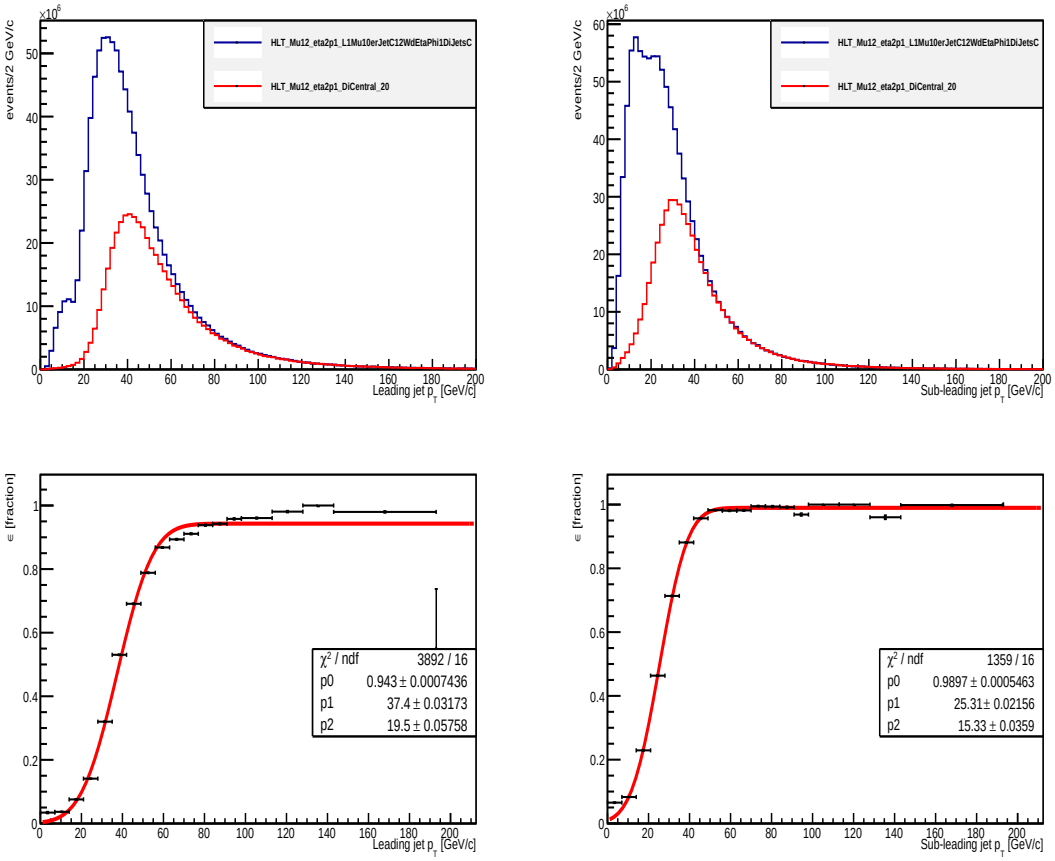

Figure 3.2: Top: reconstructed tranverse momentum distribution of the leading(left) and sub-leading(right) jet in events triggered by Mu12 (blue) and Mu12_DiJet20 (red). Bottom: trigger efficiency of Mu12_DiJet20 as function of reconstructed leading (left) and sub-leading(right) jet transverse momentum.

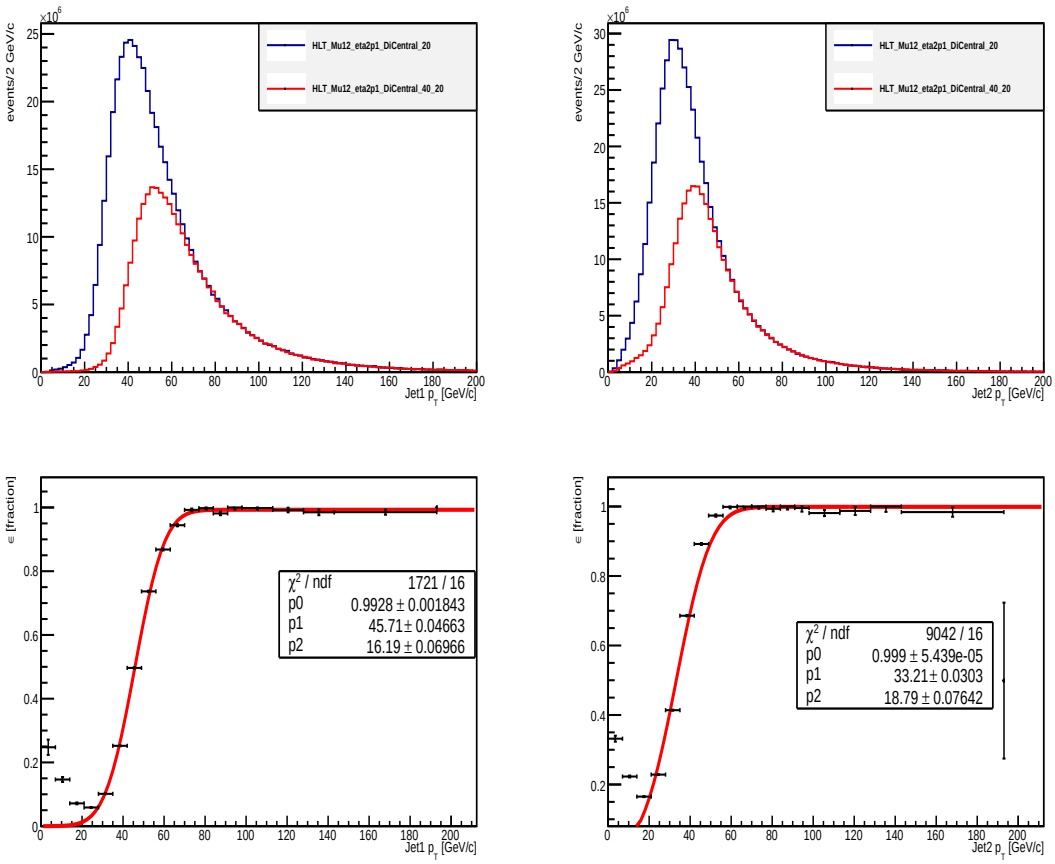

Figure 3.3: Top: reconstructed tranverse momentum distribution of the leading(left) and sub-leading(right) jet in events triggered by Mu12_DiJet20 (blue) and Mu12_DiJet40_20 (red). Bottom: trigger efficiency of Mu12_DiJet40_20 as function of reconstructed leading (left) and sub-leading(right) jet transverse momentum.

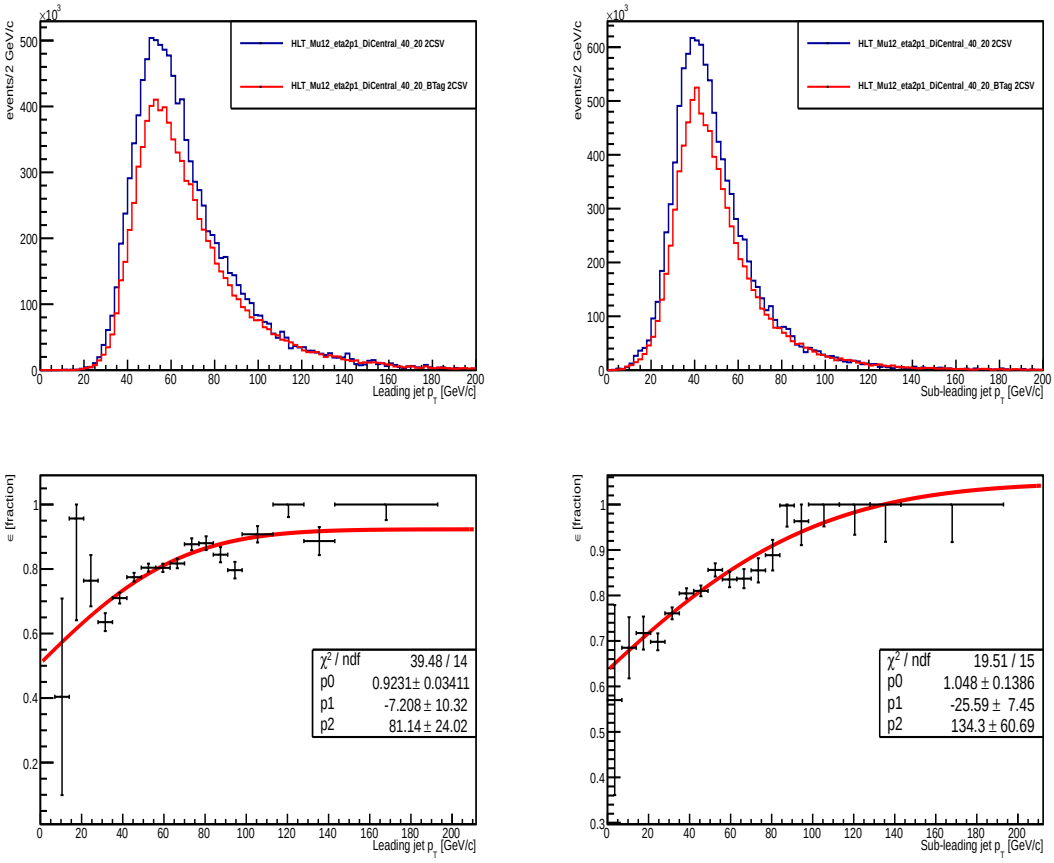

Figure 3.4: Top: reconstructed tranverse momentum distribution of the leading(left) and sub-leading(right) jet in events triggered by Mu12_DiJet40_20 (blue) and Mu12_DiJet40_20_BTag (red). Bottom: trigger efficiency of Mu12_DiJet40_20_BTag as function of reconstructed leading (left) and sub-leading(right) jet transverse momentum.

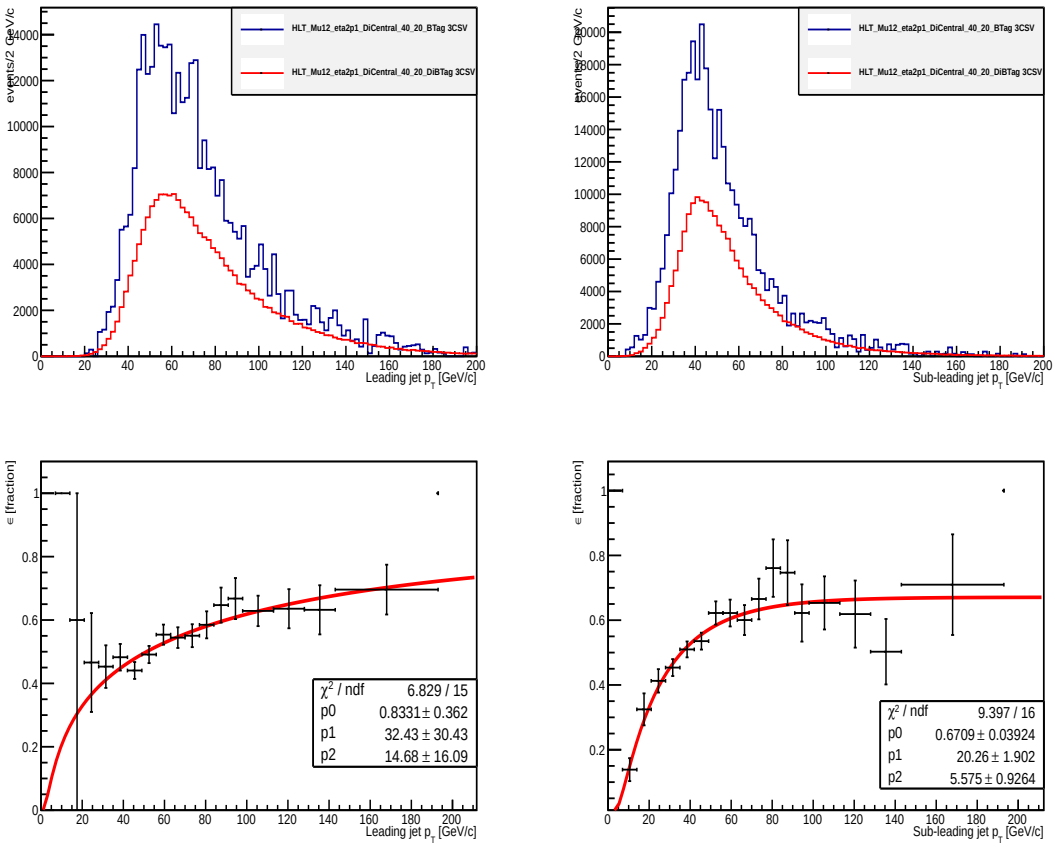

Figure 3.5: Top: reconstructed tranverse momentum distribution of the leading(left) and sub-leading(right) jet in events triggered by Mu12_DiJet40_20_BTag (blue) and Mu12_DiJet40_20_DiBTag (red). Bottom: trigger efficiency of Mu12_DiJet40_20_DiBTag as function of reconstructed leading (left) and sub-leading(right) jet transverse momentum.

Bibliography

[1] H.Nilles,"Supersymmetry, supergravity and particle physics", Physics Reports 110 (1984)

[2] CMS Collaboration,"Observation of a new boson at mass of 125 GeV with the CMS experiment at the LHC.", submitted to Physics Letters B. (2012)

[3] ATLAS Collaboration,"Observation of a new particle in the search for the Standard Model Higgs boson with ATLAS detector at the LHC.", submitted to Physics Letters B. (2012)

[4] CMS Collaboration, "The CMS experiment at the CERN LHC." *JINST*,3(08):S08004, 2008 (2008)

[5] CMS Collaboration, "Commissioning of the Particle Flow event reconstruction with the first LHC collision recorded in the CMS detector" CMS-PAS-PFT-10-001 (2010)

[6] CMS Collaboration, "Perfomance of the b-jet identification in CMS", CMS-PAS-BTV-11-001 (2011)

[7] CMS Collaboration,"Search for SuperSymmetric Higgs bsoon states decaying into $b\bar{b}$ and produced in association with b-quarks in events collected by semi-leptonic triggers in pp collision at $\sqrt{s} = 7\,\text{TeV}$", CMS PAS HIG-12-027 (2012)